

# Optical Transmission of Polymer Pillars for Chip I/O Optical Interconnections

M. S. Bakir, T. K. Gaylord, *Fellow, IEEE*, O. O. Ogunsola, E. N. Glytsis, *Senior Member, IEEE*, and J. D. Meindl, *Life Fellow, IEEE*

**Abstract**—In the pursuit of high-density wafer-level input–output optical interconnections, microscopic polymer pillars have recently been fabricated. The optical performance of these pillars is critical for their potential application to gigascale integration. In the present work, the optical transmission of these pillars is analyzed and measured. It is shown that these polymer pillars act as precision many-moded waveguides, thus, verifying the cross-sectional uniformity, smoothness of surfaces, and optical quality of the material.

**Index Terms**—Optical interconnections, polymers.

## I. INTRODUCTION

THERE IS a critical need for highly integrated wafer-level optical and electrical input–output (I/O) interconnections at the die-to-module/board level [1]–[4]. I/O interconnections between die and board have traditionally been provided by metallic conductors. Electrical interconnects, however, have inherent limitations which include high noise, high drive powers, impedance matching requirements, tradeoff between data rate and distance, insufficient densities/data rates, and expensive redesign. Optical interconnects, on the other hand, have the potential for low noise, low drive power, high density, high data rates, simplified design, and redesign. A particularly promising optical I/O technology is the recently developed sea of polymer pillars (SoPPs) [5]–[7]. It potentially has all of the above favorable optical-interconnect characteristics with the additional desirable features of low cost, high tolerance to coefficient of thermal expansion (CTE) mismatches, accommodation of wafer-level testing, and low-temperature processing compatibility with semiconductor manufacturing. Polymer pillars have also been fabricated with surface metallic conductors on them allowing simultaneous dual-mode electrical and optical interconnects [6], [7]. Furthermore, SoPPs have been fabricated at very high densities ( $> 10^5 \text{ cm}^{-2}$ ). A representative polymer pillar of Avatrel 2000P (from Promerus LLC) [8] in an array of polymer pillars made by the procedure described below is shown in Fig. 1.

However, to evaluate the potential of SoPP in practical gigascale integration, the optical performance of these pillars needs to be quantified. In this letter, the optical transmission of a representative single pillar is analyzed in Section II. The

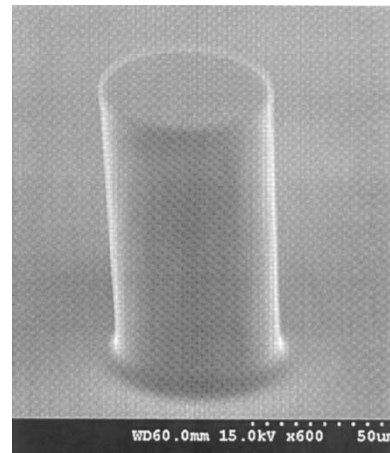


Fig. 1. Optical-interconnect polymer pillar (Avatrel 2000P)  $102 \mu\text{m}$  tall and  $55 \mu\text{m}$  diameter on a glass substrate.

fabrication of test structures is presented in Section III. The optical testing of a single pillar is described in Section IV. In the conclusions in Section V, it is shown that these polymer pillars indeed act as precision many-moded waveguides, thus, establishing their circular cross-sectional uniformity, smoothness of surfaces, and optical quality of the polymer.

## II. ANALYSIS

For optical interconnect applications, the polymer pillars are fabricated directly on semiconductor chips. The polymer pillars may be integrated with passive devices such as mirrors or grating couplers [9] or with active devices such as photodetectors or lasers. For the optical analysis and testing, polymer pillars are fabricated by the same processes, but on a glass substrate. The polymer pillar of radius  $a$  and length  $L$  is illuminated by a collimated linearly polarized light of freespace wavelength  $\lambda$  at normal incidence, as shown in Fig. 2. Under ideal circumstances, the large-diameter circular cross-sectional pillar of refractive index  $n_p$  will act like a many-moded circular waveguide. It would be similar to an optical fiber with the pillar acting as the core and air acting as the cladding. It differs from a single-mode optical fiber in that the diameter is much larger and that the cladding is air ( $n = 1$ ) rather than glass of slightly lower refractive index than the core. The general hybrid modes that are excited by the incident plane wave can be approximated by  $LP_{vm}$  modes. From symmetry, however, only the radially symmetric  $LP_{0m}$  modes are excited in the circular waveguide pillar. The electric fields of the  $LP_{0m}$  modes supported by the circular waveguide are of the form (1), shown at the bottom of

Manuscript received March 21, 2003; revised August 18, 2003. This work was performed as part of the Interconnect Focus Center research program at the Georgia Institute of Technology and was supported by MARCO and DARPA.

The authors are with the Microelectronics Research Center, School of Electrical and Computer Engineering, Georgia Institute of Technology, Atlanta, GA 30332 USA.

Digital Object Identifier 10.1109/LPT.2003.819398

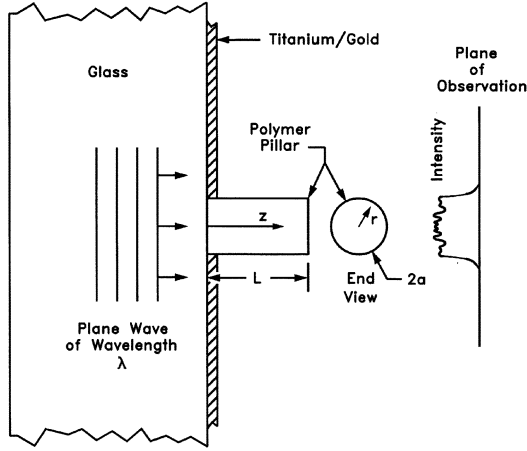


Fig. 2. Configuration for transmission analysis and experimental testing of optical-interconnect polymer pillars.

the page, where  $A_m$  is a constant ( $A_m > 0$ ) that has been adjusted so that each  $m$ th mode is normalized to the same power  $P$ . The quantity  $J_\nu$  is an integer-order ordinary Bessel function of the first kind,  $K_\nu$  is an integer-order modified Bessel function of the second kind, and  $\beta_m$  is the guided-mode propagation constant of the  $m$ th mode. The propagation constant  $\beta_m = k_0 N_m$ , where  $k_0 = 2\pi/\lambda$  and  $N_m$  is the guided-mode effective index of the  $m$ th mode. The quantities  $\kappa = k_0(n_p^2 - N_m^2)^{1/2}$  and  $\gamma_m = k_0(N_m^2 - n_p^2)^{1/2}$ . The incident wave  $E_{\text{inc}}(r)$  at  $z = 0$  launches a weighted sum of  $E_m(r)$  modes so that  $E_{\text{inc}}(r) = \sum_m C_m \varepsilon_m(r)$ . From the orthogonality condition between modes and using the Fourier-Bessel (Hankel) transform, the coefficients  $C_m$  are found to be

$$C_m = \frac{\beta_m}{2\omega\mu_0 P} \int_0^{2\pi} \int_0^\infty E_{\text{inc}}(r) \varepsilon_m^* r dr d\phi$$

$$= \sqrt{\frac{2\pi N_m}{\eta_0 P}} \cdot \frac{J_1(\kappa_m a)}{|J_1(\kappa_m a)|} \cdot \frac{E_0}{\kappa_m \sqrt{1 + (\frac{\kappa_m}{\gamma_m})^2}} \quad (2)$$

where  $\eta_0$  is the characteristic impedance of freespace,  $P$  is the reference power of each mode (taken to be 1 W), and  $E_0$  is the reference electric field (taken to be 1 V/m) of the incident wave. Due to the reflective metallization for  $r \geq a$ , the incident plane wave produces  $E_{\text{inc}}(r, \phi) = E_0 \text{rect}(r/2a)$ . The transmission of the polymer pillar at its output endface may be represented in terms of the weighted amplitudes of the numerous modes that are excited by the incident plane wave. Radiation modes are neglected. The field at the output ( $z = L$ ) is given by

$$E(r, z = L) = \sum_m C_m \varepsilon_m(r) \exp(-j\beta_m L). \quad (3)$$

At the output endface ( $z = L$ ) of the pillar, the intensity of the reflected modes are  $<4\%$  and will be neglected. The field pat-

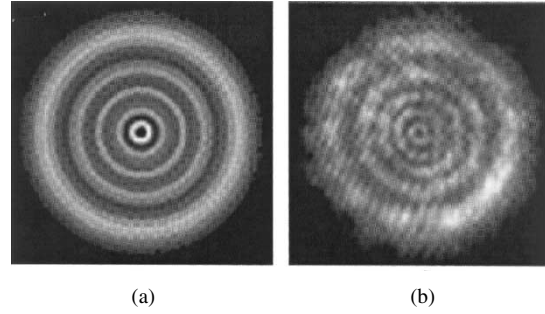


Fig. 3. Optical intensity at  $z = L + 52 \mu\text{m}$  exhibiting on-axis destructive interference (a) as calculated and (b) as experimentally measured.

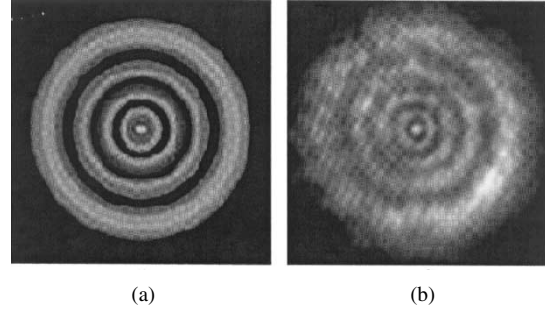


Fig. 4. Optical intensity at  $z = L + 72 \mu\text{m}$  exhibiting on-axis constructive interference (a) as calculated and (b) as experimentally measured.

tern beyond the output endface ( $z > L$ ) may be determined by propagating the fields forward to an arbitrary plane of observation ( $z$ ). The Rayleigh-Sommerfeld diffraction integral may be used for this purpose. Since there is only a radial variation in  $E(r')$  and no azimuthal variation  $\phi'$ , then the diffracted field  $E_D(r, \phi)$  will also have radial symmetry. That is,  $E_D(r, \phi) = E_D(r)$  and  $\phi = 0$  is used for simplicity. In this representation, the diffracted field  $E_D$  is given by

$$E_D(r, z > L)$$

$$= \int_{r'=0}^\infty \int_{\phi'=0}^{2\pi} \frac{\exp(-jk_0 R)}{2\pi R} \left( jk_0 + \frac{1}{R} \right) \frac{(z-L)}{R} E(r') r' dr' d\phi' \quad (4)$$

where  $r'$  and  $\phi'$  are integrated over the endface of the polymer pillar. The distance  $R$  to a point of coordinate  $r$  on the plane of observation is given by  $R = [r]^2 + r'^2 - 2r r' \cos \phi' + (z - L)^2]^{1/2}$ . This integral may be evaluated numerically using the trapezoidal rule. From the calculated  $E_D(r, z)$ , the intensity of the patterns are  $I_D(r, z) = |E_D(r, z)|^2$ . Example intensity patterns calculated in this manner using the parameters of Section III are shown in Figs. 3 and 4.

### III. FABRICATION

The fabrication of the test configuration shown in Fig. 2 is described in this section. First, 30 nm of titanium was sputtered

$$E_m(r, z) = \varepsilon_m(r) \exp(-j\beta_m z) = \begin{cases} A_m J_\nu(\kappa_m r) \exp(-j\beta_m z), & 0 \leq r \leq a \\ A_m \frac{J_\nu(\kappa_m a)}{K_\nu \gamma_m a} K_\nu(\gamma_m r) \exp(-j\beta_m z), & r \geq a \end{cases} \quad (1)$$

onto the glass. Then, 700 nm of gold was sputtered onto the titanium. Next, the titanium–gold layers were photolithographically patterned to produce vias for the polymer pillars. In this array, the center-to-center spacing between pillars was 325  $\mu\text{m}$ . Then, a very thin layer of silicon nitride was deposited to enhance the adhesion of the polymer pillars. Next, a layer of Avatrel 2000P polynorborene photopolymer was spin coated to a thickness of 102  $\mu\text{m}$  onto the prepared substrate. After soft baking, the polymer film was exposed through a mask defining the circular cross sections of the pillars. After hard baking at 100 °C for 20 min and spray developing, the polymer pillars were in place. The sample was then placed in an oven and cured at 200 °C for 2 hr. The titanium–gold film produced a reflective surface to visible light except at the location of the polymer pillars. The diameters of the pillars for the present case were  $2a = 55 \mu\text{m}$ . The refractive index of the polymer pillar was measured to be  $n_p = 1.52$  using a Woollam ellipsometer. There is great flexibility in the fabrication of the polymer pillars. They have been fabricated in other sizes and shapes including circular cross-sectional pillars 5  $\mu\text{m}$  in diameter and 12–15  $\mu\text{m}$  tall, 10  $\mu\text{m}$  in diameter and 12–20  $\mu\text{m}$  tall, 18  $\mu\text{m}$  in diameter and 12–20  $\mu\text{m}$  tall, 55  $\mu\text{m}$  in diameter and 20–170  $\mu\text{m}$  tall, elliptical cross-sectional pillars  $4 \times 12 \mu\text{m}$  and 12  $\mu\text{m}$  tall, and square cross-sectional pillars 150  $\mu\text{m}$  on a side and 100  $\mu\text{m}$  tall.

#### IV. OPTICAL TESTING

An array of polymer pillars like the structure of Figs. 1 and 2 was used for measuring the optical transmission of a pillar. An optical mask on the back side of the glass substrate blocked all of the light except that incident upon a single polymer pillar. The pillars were illuminated through the glass substrate by a collimated linearly polarized helium–neon laser of freespace wavelength  $\lambda = 632.8 \text{ nm}$ . The intensity of the transmitted light through a polymer pillar at various values of  $z$  was imaged with a  $10 \times$  microscope objective with a numerical aperture of 0.25. The images were recorded using a Sony model XC-75 charged-coupled device camera. The distances were referenced to the endface of the polymer pillar ( $z = L$ ). Intensity patterns were measured at distances of 0–1000  $\mu\text{m}$  from the pillar endface. Measured intensity patterns for  $z = L + 52 \mu\text{m}$  and  $z = L + 72 \mu\text{m}$  are shown in Figs. 3 and 4. The measured intensity pattern of Fig. 3 exhibits on-axis destructive interference and five bright rings in agreement with the calculated intensity pattern for  $z = L + 52 \mu\text{m}$ . The measured intensity pattern of Fig. 4 exhibits on-axis constructive interference and four bright rings, in agreement with the calculated intensity pattern for  $z = L + 72 \mu\text{m}$ . A total of exactly 100 modes are supported by the pillar and all  $m = 1$  to  $m = 100$  modes are included in the calculations. However, it was found that including only the first 30 modes produced essentially the same patterns. The agreement between calculations and measurements is seen to be

very good. The strong interference effects are well reproduced between the calculations and the measurements. For a distance range of 0–1000  $\mu\text{m}$  from the pillar endface, there were eight destructive interference minima along the axis of the pillar. These intensity minima occur at 7-, 17-, 32-, 53-, 83-, 133-, 234-, and 516- $\mu\text{m}$  distances ( $z - L$ ) from the pillar endface.

#### V. CONCLUSION

Microscopic optical-interconnect polymer pillars have been analyzed using mode-matching, waveguiding, and propagation methods. Polymer pillars were fabricated on glass substrates and optically tested. The optical transmission of these pillars, made of Avatrel 2000P, is in close agreement with the predicted patterns. Thus, these polymer pillars indeed act as precision many-moded waveguides. This agreement verifies the cross-sectional uniformity, smoothness of surfaces, the endface flatness, and optical quality of the material. The fact that the pillars have very smooth right-angled side walls is also apparent from Fig. 1. In addition, the polymer pillars have been shown to be highly compliant [7]. The air cladding contributes to this compliance. Simultaneously, the air cladding and the associated large refractive index discontinuity between the pillar and air, produces tightly bound guided modes. Under these circumstances, polymer pillar bending due to CTE mismatch between semiconductor die containing the pillars and substrate does not appreciably affect the transmission properties of the pillars.

#### REFERENCES

- [1] J. W. Goodman, F. I. Leonberger, S.-Y. Kung, and R. A. Athale, "Optical interconnections for VLSI systems," *Proc. IEEE*, vol. 72, pp. 850–866, July 1984.
- [2] D. A. B. Miller, "Rationale and challenges for optical interconnects to electronic chips," *Proc. IEEE*, vol. 88, pp. 728–749, June 2000.
- [3] J. D. Meindl, "The evolution of monolithic and polyolithic interconnect technology," in *IEEE Very Large Scale Integration (VLSI) Circuits Symp.*, 2002, pp. 2–5.
- [4] *International Technology Roadmap for Semiconductors (ITRS)*, Semiconductor Industry Association (SIA), 2001.
- [5] M. S. Bakir, H. A. Reed, A. V. Mulé, J. P. Jayachandran, P. A. Kohl, K. P. Martin, T. K. Gaylord, and J. D. Meindl, "Chip-to-module interconnections using 'Sea of leads' technology," *Mater. Res. Bull.*, vol. 28, pp. 61–67, Jan. 2003.
- [6] M. S. Bakir, A. V. Mulé, T. K. Gaylord, P. A. Kohl, K. P. Martin, and J. D. Meindl, "Sea of dual-mode polymer pillar I/O interconnections for gigascale integration," in *Proc. Int. Solid State Circuits Conf. (ISSCC)*, Feb. 2003, pp. 372–373.
- [7] M. S. Bakir, R. A. Villalaz, O. O. Ogunsola, T. K. Gaylord, P. A. Kohl, K. P. Martin, and J. D. Meindl, "Sea of polymer pillars: Dual-mode electrical-optical input/output interconnections," in *Int. Interconnection Technology Conf. (IITC)*, June 2003, pp. 77–79.
- [8] R. A. Shick, S. K. Jayaraman, B. L. Goodall, L. F. Rhodes, W. C. McDougall, P. A. Kohl, S. A. Bidstrup-Allen, and P. Chiniwalla, "Avatrel™ dielectric polymers for electronic packaging," *Advancing Microelectronics*, vol. 25, pp. 13–14, 1998.
- [9] S. M. Schultz, E. N. Glytsis, and T. K. Gaylord, "Design, fabrication, and performance of preferential-order volume grating couplers," *Appl. Opt.*, vol. 39, pp. 1223–1232, Mar. 2000.